Synthesis and Characterization of Lead Free Barium Strontium Titanate Dielectric Material

A dissertation submitted in the partial fulfilment of requirement for the award of the

Degree of

Masters of Science
in
Physics

Submitted by
Love Kumar
Roll No.-301004022

Under the esteemed guidance of
Dr. Dwijendra P. Singh
(Assistant Professor)

School of Physics and Materials Science
Thapar University
Patiala (Punjab)-147 004

July 2012.

Dedicated to

My Parents

CERTIFICATE

This is to certify that the Dissertation entitled **"Synthesis and Characterization of Lead free Barium Strontium Titanate Dielectric Material"** submitted by **Love Kumar (Roll No.301004022)** of M.Sc. (physics), Thapar Universty, Patiala, was carried out by him under my supervision. He has not submitted this material for credit towards any other degree at Thapar Universty, Patiala or any other Universty.

Dr. Dwijendra P. Singh

Supervisor

(Assistant Professor),

School of Physics and Materials Science,

Thapar University,

Patiala.

Dr. Kulvir Singh

(Prof. & Head)

School of Physics and Materials Science,

Thapar University,

Patiala.

Dr. S.K. Mohapatra

Dean of Academic Affairs,

Thapar University,

Patiala.

Date: 15-7-2012

Place: Thapar Universty, patiala

ACKNOWLEDGEMENT

With deep sense of gratitude, I thank all those who have contributed the conception origin and nurturing of this project.

I would like to express my sincere thanks to my project guide, ***Dr. Dwijendra P. Singh*** Assistant Professor, School of Physics and Materials Science, Thapar Universty, Patiala for providing me valuable guidance during the entire project and for providing me his timely support, help and encouragement. His guidance & suggestions were very helpful to shape my research skill. I am sure that the knowledge gained through my association with my supervisor shall go a long way in helping me to achieve goals in my life.

I would like to express my sincere regards to ***Dr. Kulvir Singh***, Professor and Head, School of Physics and Materials Science for providing me facilities without which this work would not be possible.

I would like to put my heartiest gratitude to my whole family for their constant support enthusiasm and encouragement.
I am also very much thankful to the Ph.D. scholars *Ravi Shukla, Samita Thakur, Harjinder Singh, Gaurav Singla, Pallvi Gupta, Chandani Bansal, Mintu Tyagi, Nandini Bharadwaj,Lavanya*. I am also Thankful *to Mr Purushotam* for carrying SEM and EDXS analysis on the samples.

In last but not the least I would like to thank my friends Dimple, Satwinder, Manpreet, Malti and Rohit and all those people who have helped me directly or indirectly to do my project work.

Love Kumar
Roll no: 301004022

DECLARATION

I hereby declare that the Dissertation "Synthesis and Characterization of Lead free Barium Strontium Titanate Dielectric Material" is the work carried out by me under the supervision of Dr. Dwijendra P. Singh . I have not submitted this work anywhere else for the award of any degree.

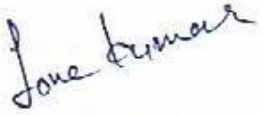

Love Kumar

Abstract

The Lead free, Barium Strontium Titanate (BST) with Different stoichiometric compositions ($Ba_{0.5}Sr_{0.5}TiO_3$, $Ba_{0.7}Sr_{0.3}TiO_3$, $Ba_{0.85}Sr_{0.15}TiO_3$) has been synthesised by Sol-Gel method. The synthesised samples have been subjected to the structural, morphological, dielectric characterisation. The X-Ray Diffraction studies have confirmed that $Ba_{0.5}Sr_{0.5}TiO_3$ and $Ba_{0.85}Sr_{0.15}TiO_3$ samples have the cubic phase while $Ba_{0.7}Sr_{0.3}TiO_3$ has tetragonal phase. The SEM studies have shown the good morphological structure and the average grain size of $Ba_{0.5}Sr_{0.5}TiO_3$ samples has been found to be 3.04 micrometre, for $Ba_{0.7}Sr_{0.3}TiO_3$ has been found to be 1.9 micrometre, for $Ba_{0.85}Sr_{0.15}TiO_3$ has been found to be 1.3 micrometre. The temperature dependence of real part of dielectric constant has confirmed the ferroelectric nature of $Ba_{0.85}Sr_{0.15}TiO_3$ samples. Moreover the dielectric constant has been found to be highest for $Ba_{0.85}Sr_{0.15}TiO_3$. But the Tangent loss is also higher for this composition. All the samples have shown the decrease of dielectric constant with increase of frequency, which is attributed the relaxing behaviour of dipoles.

TABLE OF CONTENTS

Page no.

Certificate ……...i

Acknowledgement ……ii

Declaration……...iii

Abstract ……..iv

Table of Contents…….. ……..v

Contents……vi

List of Figure.....……vii-viii

Contents

Chapter-1 Introduction

1.1 Introduction and Motivation….....1

1.2 Perovskite Crystal Structure …….....2

1.2.1 Barium Strontium Titanate Crystal Structure …….....3

1.3 Effect of temperature and Phase transition …….....4

1.3.1 Ehrenfest classification of Phase Transition 6

1.3.2 Modern classifications of phase transitions.....8

1.4 Variation of dielectric constant with frequency.....8

1.5 Loss Tangent.....10

Chapter-2 Experimental Details

2.1 Characterization Techniques.....11

2.1.1 X-Ray Diffraction (XRD).....11

2.1.2 Energy dispersive X-ray spectroscopy (EDXS)…….13

2.1.3 Scanning Electron Microscope (SEM)……15

2.1.4 Dielectric Measurements…….....17

2.2 Synthesis.....18

2.2.1 Sol-Gel Method…….18

2.2.1.1 Sol-Gel Chemistry…….19

2.2.2 Preparation of sample……21

Chapter-3 Results and Discussion

3.1 XRD Analysis……..…23

3.2 SEM Analysis……...26

3.3 Electron Dispersive X-ray Spectroscopy analysis…..28

3.4 Dielectric Measurements……..….29

Chapter-4 Conclusions and Future Scope

4.1 Conclusions ……..….....35

4.2 Future Scope.....36

References……37-38

LIST OF FIGURE

Fig. 1.1. Pervoskite crystal structure.

Fig. 1.2. Elements occupying A and B positions in Pervoskite structure.

Fig. 1.3. BST crystal structure in cubic phase with no external applied field.

Fig.1.4. Phase transitions and corresponding changes in crystal structure of perovskite ferroelectric materials.

Fig.1.5. Variation of dielectric constant with frequency.

Fig.2.1. Bragg's Law Reflection.

Fig.2.2. XRD apparatus.

Fig.2.3. Schematic diagram of inner atomic electron shell.

Fig.2.4. Schematic of SEM.

Fig.2.5. Principle of SEM.

Fig.2.6. Schematic representation of Sol-Gel process for synthesis of nanoparticles.

Fig.3.1. XRD analysis of (a) $Ba_{0.5}$ $Sr_{0.5}$ TiO_3 (b) $Ba_{0.7}$ $Sr_{0.3}$ TiO_3 (c) $Ba_{0.85}$ $Sr_{1.5}$ TiO_3.

Fig.3.2. SEM (Scanning Electron Microscope) micrograph images of (a) $Ba_{0.5}Sr_{0.5}TiO_3$ (b) $Ba_{0.7}Sr_{0.3}TiO_3$ (c) for $Ba_{0.85}Sr_{0.15}TiO_3$.

Fig. 3.3 EDXS Spectrum of (a) $Ba_{0.5}Sr_{0.5}TiO_3$ (b) $Ba_{0.85}Sr_{0.15}TiO_3$.

Fig.3.4. Variation of dielectric constant with frequency for different compositions.

Fig.3.5. Variation of Loss Tangent with frequency for different composition.

Fig.3.6. Variation of dielectric constant with temperature at different frequency For $Ba_{0.5}Sr_{0.5}TiO_3$.

Fig.3.7 Variation of dielectric constant with temperature at different frequency For $Ba_{0.7}Sr_{0.3}TiO_3$.

Fig.3.8.Variation of dielectric constant with temperature at different frequency For $Ba_{0.85}Sr_{0.15}TiO_3$.

CHAPTER 1

Introduction

1.1 Introduction and Motivation

Barium Titanate is an inorganic ferroelectric material with excellent dielectric properties to be used in devices. In the recent years, the researchers have put lots of effort, time and money on ferroelectric materials. The driving force behind this interest is the 250 billion dollar semiconductor industry, which is rising at a good rate [1, 3].

There is a rush to get the improved, more efficient, non-hazardous (i.e. lead free) materials for industry to be used in devices. To gain this momentum, either we should search for new materials or should fabricate the existing materials to get desired properties.

The dependence of dielectric permittivity on the applied electric field, low loss tangent, high dielectric constant and low cost of processing makes barium strontium titanate (BST) a promising ferroelectric material for applications in tunable microwave devices such as phase shifters and filters. High tunability and low dielectric loss is desired for tunable microwave devices [1-5]. The primary objective of this work was to optimize the tunability and dielectric loss of BST at microwave frequencies with different compositions. In this project, barium Strontium Titanate $(Ba_{0.5}Sr_{0.5})TiO_3$ (BST), $(Ba_{0.7}Sr_{0.3})TiO_3$ (BST) and $(Ba_{0.85}Sr_{0.15})TiO_3$ (BST) were fabricated and studied.

1.2 Pervoskite Crystal Structure

The mineral perovskite ($CaTiO_3$) is named after a Russian mineralogist, Count Lev Aleksevich von Perovski. It was discovered and named by Gustav Rose in 1839 from samples found in the Ural Mountains. The perovskite-like structure, named after the $CaTiO_3$ perovskite mineral , is a ternary compound of formula ABO_3 where A and B cations differ in size. It is considered a FCC- derivative structure in which the larger A cation and oxygen together form an FCC lattice, on the other hand the smaller B cation occupies the octahedral interstitial sites in the FCC array [6,7].

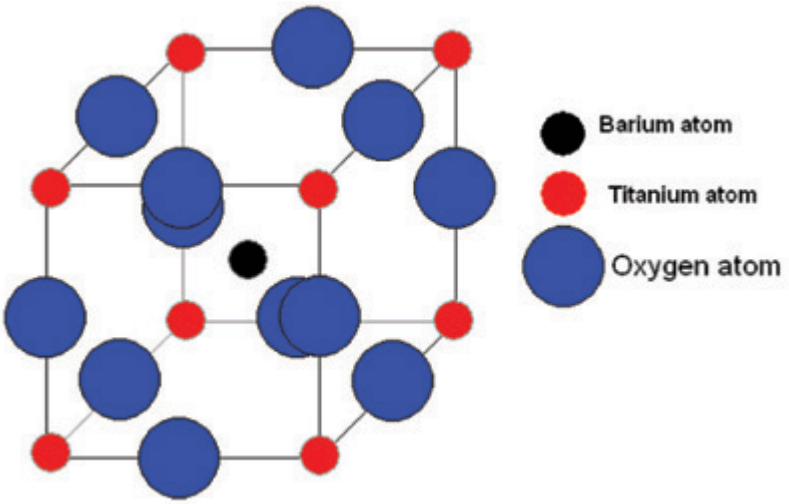

Figure 1.1: Pervoskite crystal structure

The traditional view of the perovskite lattice is that it consists of small B cations within oxygen octahedra, and larger A cations which are XII fold coordinated by oxygen. The ions occupying the A and B lattice sites are detailed in Figure 1.2

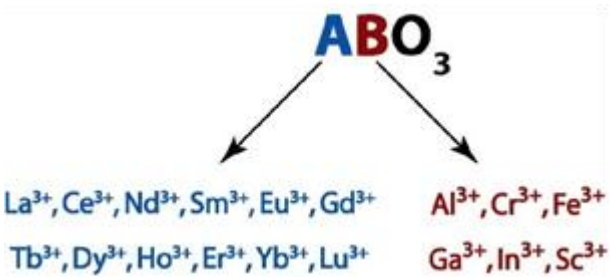

Figure 1.2: Elements occupying A and B positions in Pervoskite Structure

The coordination number of A (Ba^{+2} Barium) is 12, while the coordination number of B (Ti^{+4} Titanium) is 6. In fact, any structure consisting of the corner-linked oxygen octahedra with a small cation filling the octahedral hole and a large cation (if present) filling the dodecahedral hole is usually regarded as a perovskite, even if the oxygen octahedra are slightly distorted. Also, it is unnecessary that the anion is oxygen. For example, fluoride, chloride, carbide, nitride, hydride and sulfide perovskites are also classified as the perovskite structures. As a result, we can say that perovskite structure has a wide range of substitution of cations A and B, as well as the anions, the substitution must maintain charge balance and keep sizes within the range for particular coordination number. Because the variation of ionic size and small displacements of atoms that lead to the distortion of the structure and the reduction of symmetry have profound effects on physical properties, perovskite structure materials play such an important role in dielectric ceramic [6-9].

1.2.1 Barium Strontium Titanate Pervoskite Crystal Structure

In BST (Barium strontium titanate) also belongs to pervoskite structure family where Barium and Strontium occupy corners of cube and are shared between 8 adjacent cells as shown in following fig.1.3.

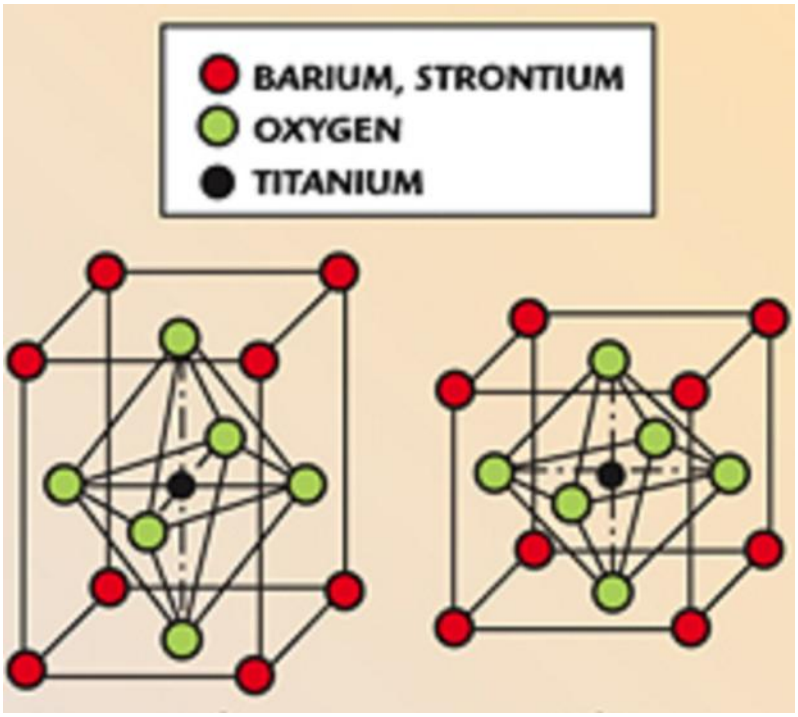

Figure 1.3: BST crystal structure in cubic phase with no external applied field

BST crystals exit both in cubic and tetragonal symmetry depending upon (Ba/Sr) ratio and correspondingly the Curie temperature depends on this ratio.

1.3 Effect of temperature and the Phase Transition

Below the curie temperature, the position of Ti ion is at the off centre position giving rise to the formation of permanent dipoles. These dipoles are ordered, giving a domain structure with a net spontaneous polarization within the domain. Above Curie temperature, the thermal energy is sufficient to allow the Ti atoms to move randomly from one position to another and so there is no fixed asymmetry. The open octahedral site allows the Ti atom to develop a large dipole moment in an applied electric field, but there is no spontaneous alignment of the dipoles in a particular direction. In this symmetric configuration material is paraelectric. The crystallographic phase change associated with BTO unit cell is depicted in Figure 1.4

The phase transition behaviour of ferroelectrics is theoretically modelled using the Landau-Ginzburg-Devonshire (LGD) theory [6, 7, 10, 11].

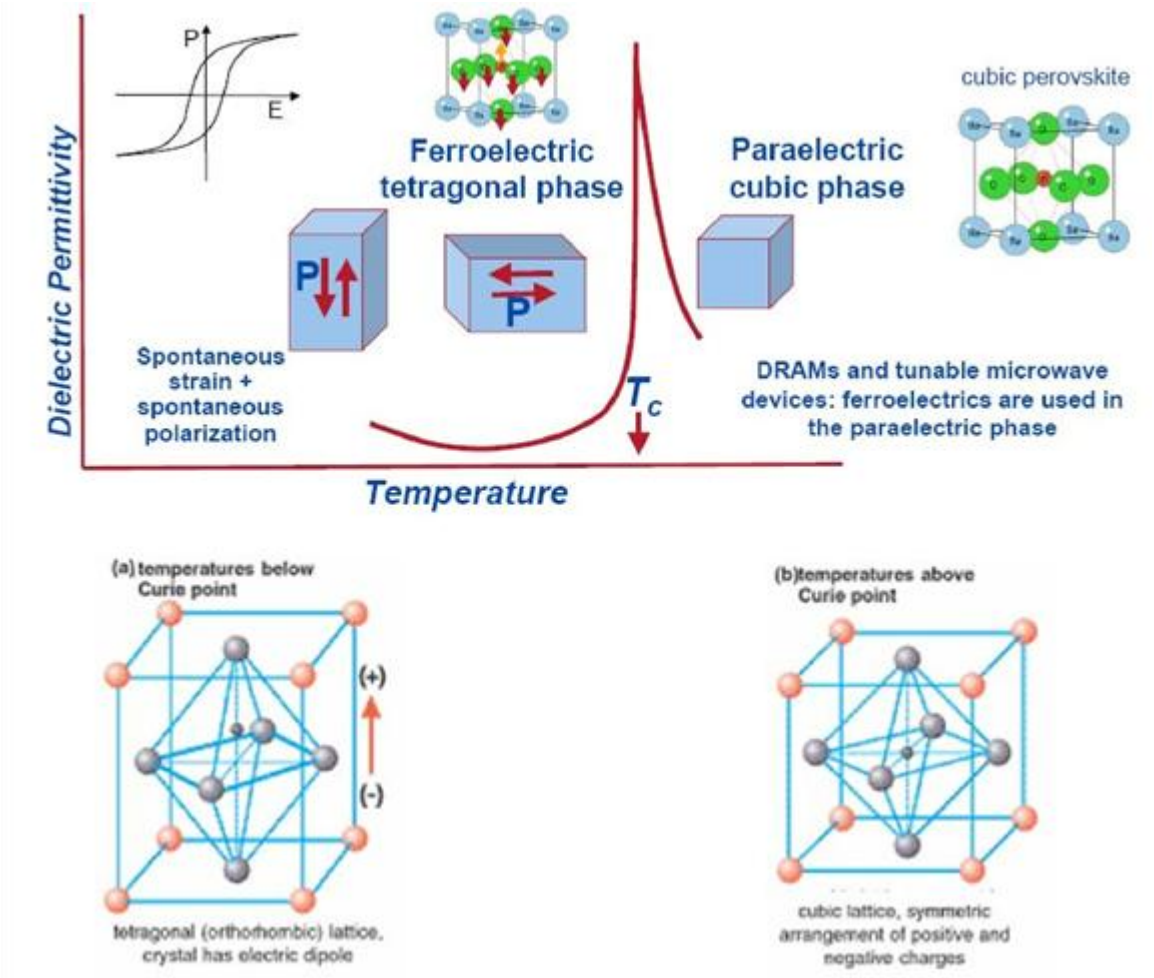

Figure 1.4: Phase transitions and corresponding changes in crystal structure of perovskite ferroelectric materials.

As depicted in fig.1.4 in the ferroelectric phase, the dielectric constant increases as the temperature increases.

While in the paraelectric phase, the dielectric constant decreases with increase in temperature obeying the Curie-Weiss law. The Curie-Weiss law is given as follows:

$$x = \frac{C}{T - T_c}$$

Where $\mathcal{E}_r$ is the dielectric permittivity, T_c measured in kelvin, T is absolute temperature. Below T_c there is spontaneous polarisation. [12-14].

Phase transitions in perovskite ferroelectric crystals is associated with a change in crystal structure from non-centro symmetric polar lattice (paraelectric) to a centro symmetric non-polar (paraelectric phase). In the ferroelectric phase, adjoining dipoles align themselves in a particular direction forming regions of local alignment called domains. The alignment gives a net dipole moment to the domain and thus a net polarization called as spontaneous polarization (P_s). Domains are formed due to stray electric fields which are created by non-compensated polarization charges. However the direction of polarization in the neighbouring domains is not the same; hence the ferroelectric material displays no overall polarization unless an electric field is applied to it. The domains are separated by domain walls and a particular domain pattern is a result of stresses created at the Curie point, uncompensated surface charges and physical imperfections (vacancies, dislocations and dopants).

1.3.1 Ehrenfest classification of Phase Transition

Paul Ehrenfest classified phase transitions based on the behaviour of the thermodynamic free energy as a function of other thermodynamic variables. Under this scheme, phase transitions were labelled by the lowest derivative of the free energy that is discontinuous at

the transition as first order and second order phase transitions.

Though useful, Ehrenfest's classification has been found to be an inaccurate method of classifying phase transitions, for it does not take into account the case where a derivative of free energy diverges (which is only possible in the thermodynamic limit). For instance, in the ferromagnetic transition, the heat capacity diverges to infinity.

First order phase transitions

In First-order phase transitions, the first derivative of the free energy with respect to some thermodynamic variable is discontinuous. The various solid/liquid/gas transitions are classified as first-order transitions because they involve a discontinuous change in density, which is the first derivative of the free energy with respect to chemical potential.

Second-order phase transitions

The first derivative (the order parameter, which is the first derivative of the free energy with respect to the external field, is continuous across the transition) is continuous but exhibit discontinuity in a second derivative of the free energy. These include the ferromagnetic phase transition in materials such as iron, where the magnetization, which is the first derivative of the free energy with respect to the applied magnetic field strength, increases continuously from zero as the temperature is lowered below the Curie temperature. The magnetic susceptibility, the second derivative of the free energy with the field, changes discontinuously. Under the Ehrenfest classification scheme, there could in principle be third, fourth, and higher-order phase transitions.

1.3.2 Modern classifications of Phase Transitions

In the modern classification scheme, phase transitions are divided into two broad categories, named similarly to the Ehrenfest classes:

First-order phase transitions are those that involve a latent heat. During such a transition, a system either absorbs or releases a fixed (and typically large) amount of energy. During this process, the temperature of the system will stay constant as heat is added: the system is in a "mixed-phase regime" in which some parts of the system have completed the transition and others have not. Familiar examples are the melting of ice or the boiling of water (the water does not instantly turn into vapour, but forms a turbulent mixture of liquid water and vapour bubbles).

Second-order phase transitions are also called continuous phase transitions. They are characterized by a divergent susceptibility, an infinite correlation length, and a power-law decay of correlations near criticality. Examples of second-order phase transitions are the ferromagnetic transition, superconductor (latent heat included when in magnetic field, need further edit) and the superfluid transition. Lev Landau gave a phenomenological theory of second order phase transitions [12].

1.4 Variation of dielectric constant with frequency

Dielectric constant is the measure of the resistance that is encountered when forming an electric field in a medium. So, permittivity is a measure of how an electric field affects, and is affected by, a dielectric medium. The permittivity of a medium describes how much electric field (more correctly, flux) is 'generated' per unit charge in that medium. Less electric flux exists in a medium with a high permittivity (per unit charge) because of polarization effects.

There is a decrease of ε' with increase in frequency. This decrease of dielectric constant with increase in frequency is up to around 10 kHz, beyond which it almost remains constant. At low frequencies electronic, ionic, dipolar and interfacial/surface polarizations contribute to the total value of dielectric constant, but for frequencies above 10 kHz the contribution from interfacial/surface polarization gets minimized. The interfacial/surface polarization can be explained by using a Maxwell-Wagner mechanism and a Shockley-Read mechanism. The Maxwell-Wagner mechanism was concerned with interfacial polarization due to ionic motion in presence of an electric field [6,7,15].

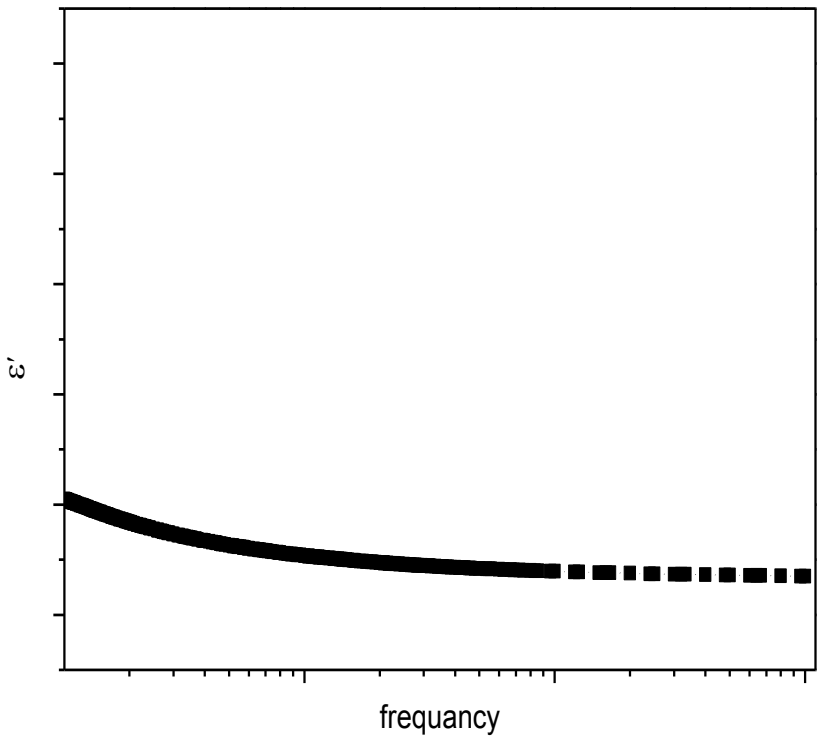

Figure 1.5: Variation of dielectric constant with frequency

1.5 Loss Tangent

The loss tangent is a parameter of a dielectric material that quantifies its inherent dissipation of electromagnetic energy. The fundamental reason of loss is the interaction of ac field with the phonons of material. Mathematically loss tangent is given by

$$\tan\delta = \frac{\varepsilon''}{\varepsilon'} << 1$$

Where Ɛ′′ and Ɛ′ are the ac and dc variations of dielectric permittivity [16].

Loss Tangent should be low for dielectric material.

CHAPTER 2

Experimental Details

2.1 Characterization Techniques

Success in devising and collecting systems on the scale of nanometers require a deeper understanding of the basic processes and phenomena involved. Hence, one of the current key objectives is to adapt and develop a range of techniques that can characterize the structural, thermal, electronic, magnetic, dielectric, composition, electrical and optical properties of the nanostructured systems. These techniques include X-Ray Diffraction, Scanning Electron Microscope (SEM), Energy Dispersive X-Ray Spectroscope (EDAX), Dielectric measurements.

2.1.1 X-Ray Diffraction (XRD)

In X-ray diffraction or scattering (XRD), X-ray photons are utilized to probe the matter. The energy of the emitted radiation is specific for each element. X-rays were discovered by Roentgen, he called them X-rays because their nature at first was unknown so, X-rays were also called Roentgen rays. The X-rays lie in the range of $0.1\ Å < \lambda < 1000\ Å$. The penetrating power of X-rays depends on energy.

Principle

X-Ray diffraction effects are observed when electromagnetic radiation impinges on periodic structures with geometrical variations comparable to the length scale of the wavelength of the radiation. X-ray diffraction is based on constructive interference of monochromatic X-rays and a crystalline sample. These X-rays are generated by a cathode

ray tube, filtered to produce monochromatic radiation, collimated to concentrate and directed towards the sample. X-rays are generated when high velocity electrons impinge on a metal target. Approximately 1% of the total energy of the electron beam is converted into X-ray radiation. In order to get a narrow beam of X-rays, the X-rays generated by the target material are allowed to pass through a collimator which consists of two sets of closely packed metal plates separated by a small gap. The collimator absorbs all the X-rays except the narrow beam that passes between the gaps[17,18].

Bragg's Law

Bragg's Law is generally used for investigating the internal structures and crystal structures of different solid compounds fig.2.1 shows the diffraction of X-ray beam according to Bragg's law. The general relationship between wavelengths of the incident X-rays, angle of incident and spacing between the crystal lattice planes of atoms is known as Bragg's law, as given by Eq. (1).

$$n\lambda = 2d\sin\theta \quad \ldots\ldots\ldots\ldots\ldots\ldots\ldots\ldots\ldots\ldots (1)$$

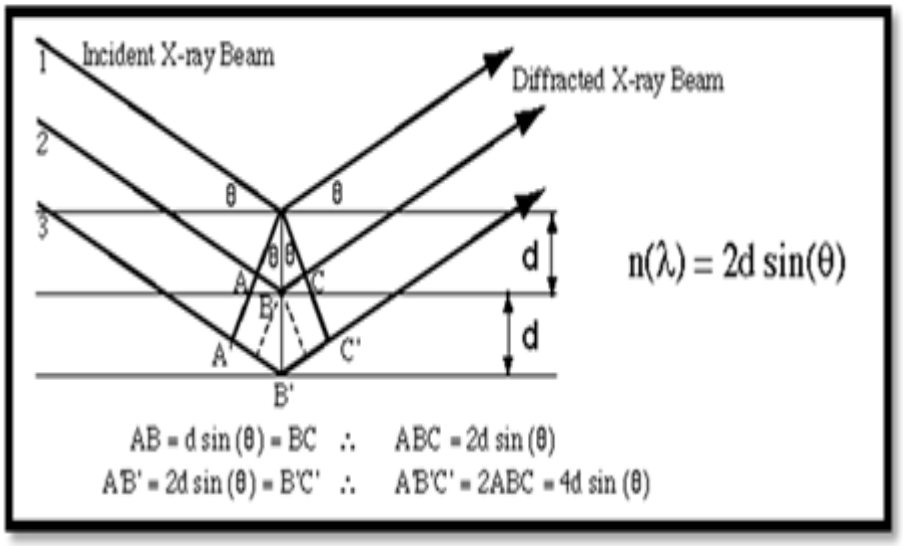

Figure 2.1: Bragg's Law Reflection

Where d is the spacing between atomic planes in the crystalline phase and λ is the X-ray wave length. The intensity of the diffracted X-rays is measured as a function of the diffraction angle 2θ and the specimen's orientation.

Diffraction peak positions are accurately measured with XRD, which makes it the best method for characterizing homogeneous and inhomogeneous strains. Inhomogeneous strains vary from crystallite to crystallite or within a single crystallite and this causes a broadening of the diffraction peaks that increases with the sine of the angle (θ) [18,19].

Figure 2.2: XRD apparatus

2.1.2 Energy dispersive X-ray spectroscopy (EDXS)

The fundamental of the EDS technique is by making the use of the X-ray spectrum and emitted by a solid sample bombarded with a focused beam of electrons to obtain a localized chemical analysis. In the periodic table it show all elements starting from atomic number 4 (Be) to 92 (U) can be detected in principle, though not all instruments are equipped for 'light' elements (Z < 10). Qualitative analysis consists of the identification of the lines in the

spectrum and is fairly straightforward owing to the simplicity of X-ray spectra. During this process, the sample preparation of the electron probe analyses only to a shallow depth, specimens should be well polished so that surface roughness does not affect the results.

It's important to know the atomic structures are according to the Rutherford-Bohr model of the atom is that the electrons orbit around the positive nucleus. In the case of the normal state, the number of orbital electrons equals the number of protons in the nucleus (given by the atomic number, Z). Only certain orbital states with specific energies exist and these are defined by quantum numbers. With increasing Z, orbits are occupied on the basis of minimum energy, those nearest to the nucleus are the most tightly bound, being filled first. This model of the inner structure of the atom is illustrated in fig.2.3. The populations of the inner shells are governed by the Pauli Exclusion Principle.

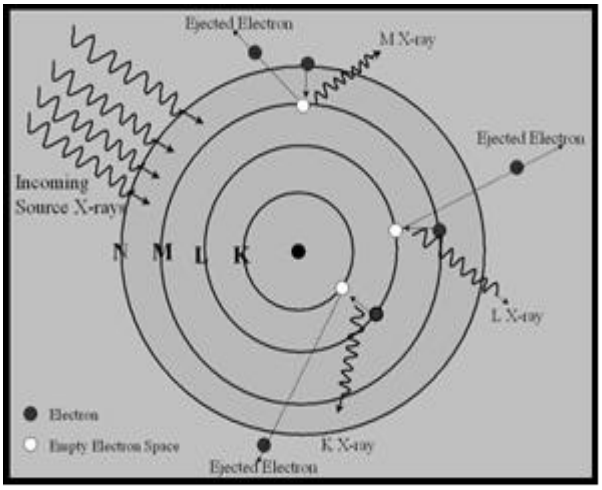

Figure 2.3: Schematic diagram of inner atomic electron shell.

The characteristic X-rays result from electron transitions between inner orbits, which are normally full. An electron must first be removed in order to create a vacancy into which another can fall from an orbit lying farther [21].

2.1.3 Scanning Electron Microscope (SEM)

SEM is a technique that uses electrons as a substitute of light to form an image. Since their development in the early 1950's, SEM has allowed researchers to examine a much bigger variety of specimens. SEM has a large depth of field, which allows more of a specimen to be in focus at one time, SEM also has much higher resolution, so closely spaced specimens can be magnified at much higher levels. Because SEM uses electromagnets rather than lenses, the researcher has much more control in the degree of magnification. It is an instrument that

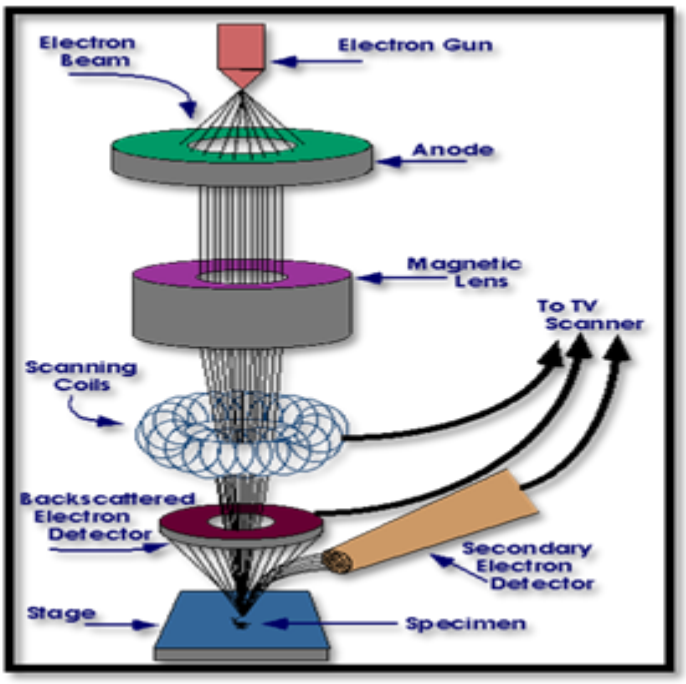

Figure 2.4: Schematic of SEM.

produces a largely magnified image by using electrons instead of light to form an image. A beam of electrons is produced at the top of the microscope by an electron gun and the electron beam follows a vertical path through the microscope, which is held within a vacuum, the beam travels through electromagnetic fields and lenses, which focus the beam down towards the sample. Once the beam hits the sample, electrons and X-rays are ejected from the sample, as

can be observed in fig.2.4. The detectors collect these X- rays, backscattered electrons, and secondary electrons and convert them into a signal that is sent to a screen similar to a television screen, which produces the final image . It is generally of non – destructive nature, though sometimes it can cause sample damage due to high energy electron beam irradiation.

Principle of SEM

When an electron beam bombards a solid surface, the incident electrons are scattered. The electron scattering can be divided into two categories, elastic and inelastic scattering, but the speed remains constant. Hence, the kinetic energy of the incident electron remains the same. During an inelastic event, part of the energy of the incident electron is transferred to its colliding partner. Secondary electron, Auger electrons and X-ray are produced by the inelastic scattering events, as shown in fig.2.5.

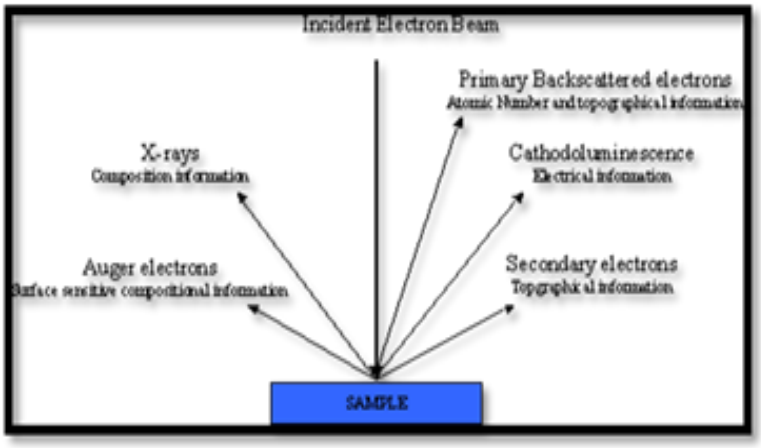

Figure 2.5: Principle of SEM.

Secondary electrons (SEs)

These are defined as electrons emitted from the specimen at less than 50eV. They are predominantly produced by the interactions between energetic electrons and weakly bonded

valence electrons of the specimen. The secondary electron peak typically show a most probable energy of 2-5eV [19,20].

2.1.4 Dielectric Measurements

Dielectric measurement was performed on the sintered pellets to find the frequency and temperature dependence of dielectric parameters such as real and imaginary part of dielectric constant, loss tangent. For this purpose Fluke PM6306 programmable automatic RCL (resistor capacitor inductor) meter was used.

2.2 Synthesis

There are many methods for the fabrication of ceramics for example solid state method, precipitation method, chemical vapour method and sol-gel method. Out of these, sol-gel method has many advantages over other methods and was chosen for the fabrication of Barium Strontium Titanate.

2.2.1 Sol-Gel Method

The sol-gel process is a wet chemical technique widely used in the field of material science and ceramic engineering. Such methods are used primarily for the fabrication of materials (typically a metal oxide). The sol-gel process, as the name implies, involves the evolution of inorganic networks through the formation of a colloidal suspension (sol) and gelation of the sol to form a network in a continuous liquid phase (gel). The starting material is processed to form a dispersible oxide and forms a sol in contact with water or dilute acid. During the process, the sol yields the gel, and the sol/gel transition controls the particle size and shape. Sol-gel processing refers to the hydrolysis and condensation of alkoxide-based precursors. The

reactions involved in the sol-gel chemistry is based on the hydrolysis and condensation of metal alkoxides M (OR), it can be described as follows:

$$MOR + H_2O \rightarrow MOH + ROH \text{ (hydrolysis)}$$

$$MOH + ROM \rightarrow M\text{-}O\text{-}M + ROH \text{ (condensation)}$$

The sol-gel process can be characterized by a series of distinct steps:

- The first step consists of the formation of different stable solutions of the alkoxide or solvated metal precursor (the sol).
- In the second step, gelation begins, which results in the formation of an oxide - or alcohol - bridged network (the gel) by a poly-condensation or poly-esterification reaction that results in a dramatic increase in the viscosity of the solution.
- The third step is the aging of the gel, during which the poly-condensation reactions continue until the gel transforms into a solid mass, accompanied by contraction of the gel network and expulsion of solvent from gel pores. It is referred to as coarsening, phenomenon by which smaller particles are consumed by larger particles during the growth process and phase transformations may occur concurrently with syneresis.
- The fourth step is drying of the gel, when water and other volatile liquids are removed from the gel network. This process is complicated due to fundamental changes in the structure of the gel. The drying process has itself been broken into four distinct steps: (i) the constant rate period, (ii) the critical point, (iii) the falling rate period, (iv) the second falling rate period. If isolated by thermal evaporation, the resulting monolith is termed a xerogel. If

the solvent (such as water) is extracted under supercritical or near super critical conditions, the product is an aerogel.

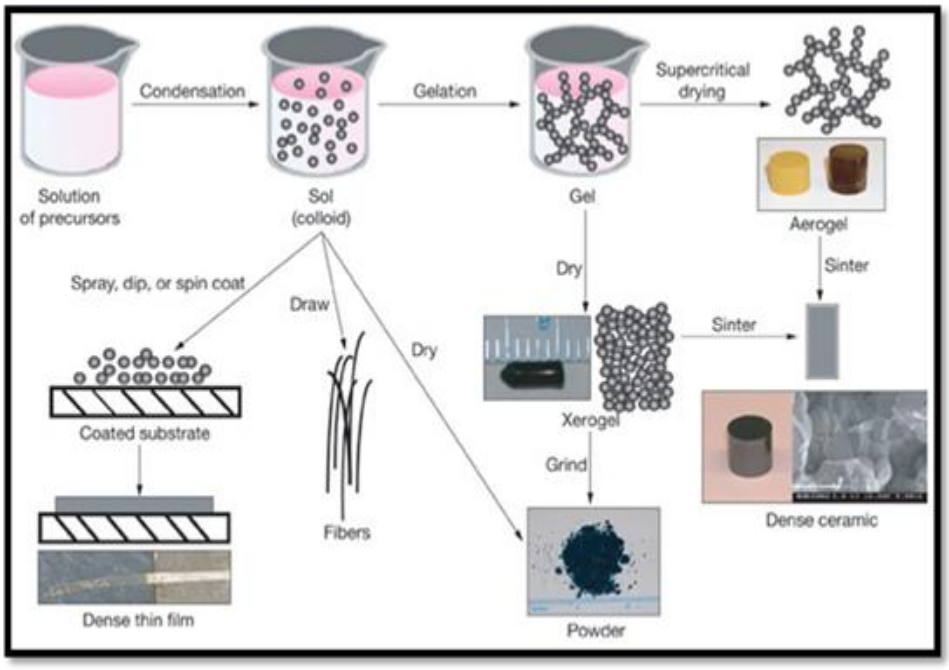

Figure 2.6: schematic representation of Sol-Gel process for synthesis of Nanoparticles.

- The fifth step involves dehydration, during which surface - bound M-OH groups are removed, thereby stabilizing the gel against rehydration.
- Thermal treatment: calcination and sintering.

2.2.1.1 Sol-Gel Chemistry

The selection of precursors (i.e. starting compound) is very important in sol-gel process. The ideal compound to be used as precursor should satisfy the following criteria:

- It should have high metal content: To minimize the volume change during the change from metal-organic solution to inorganic powder.
- High solubility in common solution with other starting compounds.

- It should be chemically compatible with other compounds.
- Cost effective to produce: as the capital equipment requirments are small (e.g. no high vacuum systems are needed), so the cost of sol-gel process is low, and precursor should not change this advantage.
- Thermally decompose without evaporating, melting or leaving carbon content.

Selection of solution

- Solutions have high vaporization rates: they should evaporate as early as possible. Vaporization depends on vapour pressure and interaction between solute and solvent.
- Solvent must be carefully be selected in order to get solution of high concentration of necessary components, proper viscosity and proper surface tension.

Advantage of sol-gel processing

- Can have low temperature sintering capability, usually 200-600°C.
- Can produce thin bond-coating to provide excellent adhesion between the metallic substrate and top.
- Can provide a simple, economic and effective method to produce high quality coatings.
  .
- Can produce high purity products because the organo-metallic precursor of the desired ceramic oxides can be mixed, dissolved in a specified solvent and hydrolyzed into a sol, and subsequently a gel, the composition can be highly controllable.
- Can provide a simple, economic and effective method to produce high

Quality coatings [22,23].

Disadvantage of sol-gel processing

- Long processing times.
- Serious health hazards of organic solutions.
- Large Shrinkage during processing.
- Easy cracking during drying stage.

2.2.2 Preparation of sample

The $Ba_xSr1\text{-}xTiO3$ solutions with compositions x=0.5, 0.7, 0.85 were produced.

Specification of chemicals

The precursors for first solution are Barium Acetate, $Ba(CH_3COO)_2$ (Sigma Aldrich, 99%) and Strontium Acetate, $Sr(CH_3COO)_2$ (Sigma Aldrich, 97%) and Acetic acid was used as the solvent, CH_3COOH (Sigma Aldrich, 99%). For second Precursor solution Titanium (iv) isopropoxide, Ti $(C_3H_7O)_4$ (Sigma Aldrich, 97%) and methoxyethanonol (Sigma Aldrich, 97%) was used as the solvent. Acetyl acetone (Sigma Aldrich) was used the stabilizer.

Solution preparation

The solution preparation method is adapted from Dien et al [25]. First Barium acetate and Strontium acetate were dissolved in Acetic acid at room temperature separately, with acetic acid: acetate molar ratio 25:1. The solutions were stirred by magnetic stirrer at 70^oC for 40 min. separately. Then after heating these solutions were mixed. In another beaker Ti

(iv) isopropoxide was dissolved in 2-methoxyethanol in molar ratio of 2-methoxyethanol: Ti(iv) isopropoxide = 30:1. This solution was also stirred on magnetic stirrer at 70^{o}C.

Then two solutions were mixed to get the parent solution. The parent solution was now diluted with acetic acid with ratio of acetic acid: Ti(iv) isopropoxide = 80:1. This solution was remained as it is for 18 hours at room temperature. After that it was heated at 90^{o} C on magnetic stirrer along with slow stirring until we got the powder form. Then it was calcined at 200^{o} C for 5 hours. Then it was grinded for around 20 minutes with Mortar Pestle. Then this powder was sintered at 700^{o} C for five hours in the Pitt furnace. Then pellets were made with help of die punch machine. These pellets were sintered again at 700^{o} C. Then the various measurements were done.

CHAPTER 3

Results and Discussion

The structural, morphological and elemental analysis is carried out by using XRD, SEM and EDS respectively. The dielectric studies has also been done. The Results of these experimental investigations are discussed in the subsequent subsection.

3.1 XRD Analysis

Fig. 3.1 (a) shows the XRD diffractogram of $Ba_{0.5}Sr_{0.5}TiO_3$ nanoparticles, where all the major peaks are indexed and well- matched to the cubic structure with cell parameters a = b = c = 3.991Å (0.6 % error) (File No. 34-0411). The crystallite size of synthesized nanoparticles was calculated by Scherer's formula, as given below:-

$$d = \frac{k\lambda}{\beta \cos \theta}$$

where k is the shape factor (k = 0.94), λ is the x-ray wavelength, β is the line broadening at half the maximum intensity (FWHM) in radians, and θ is the Bragg angle, d is the crystallite size. The crystallite size for $Ba_{0.5}Sr_{0.5}TiO_3$ nanoparticles was found to be 17.233nm.

fig.3.1(b) shows the XRD diffractogram of $Ba_{0.7}Sr_{0.3}TiO_3$ nanoparticles, where all the major peaks are indexed and well- matched to the tetragonal structure with cell parameters a = b =3.979087(0.16% error) c = 3.97093Å (File No. 89-0274). The crystalline size of $Ba_{0.7}Sr_{0.3}TiO_3$ was found using Scherer's formula to be 28.39029 nm

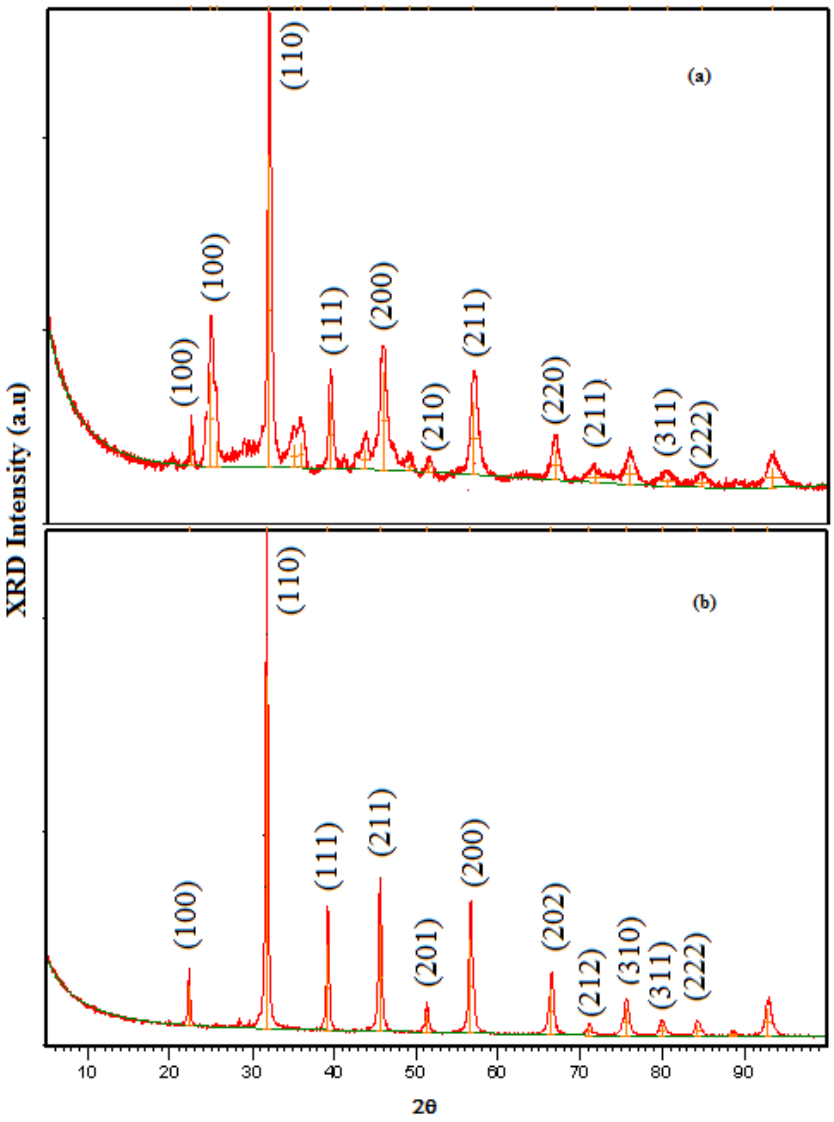

Figure 3.1: XRD diffravtogram of (a) $Ba_{0.5}$ $Sr_{0.5}$ TiO_3 (b) $Ba_{0.7}$ $Sr_{0.3}$ TiO_3

fig.3.1 (c) shows the XRD diffractogram $Ba_{0.85}Sr_{0.15}TiO_3$ of nanoparticles, where all the major peaks are indexed and well- matched to the the cubic structure with cell parameters a = b = c = 3.9916 Å (0.67 % error) (File No. 34-0411). The crystalline size of $Ba_{0.85}Sr_{0.15}TiO_3$ nanoparticle was found using Scherer's formula to be 23.39029 nm.

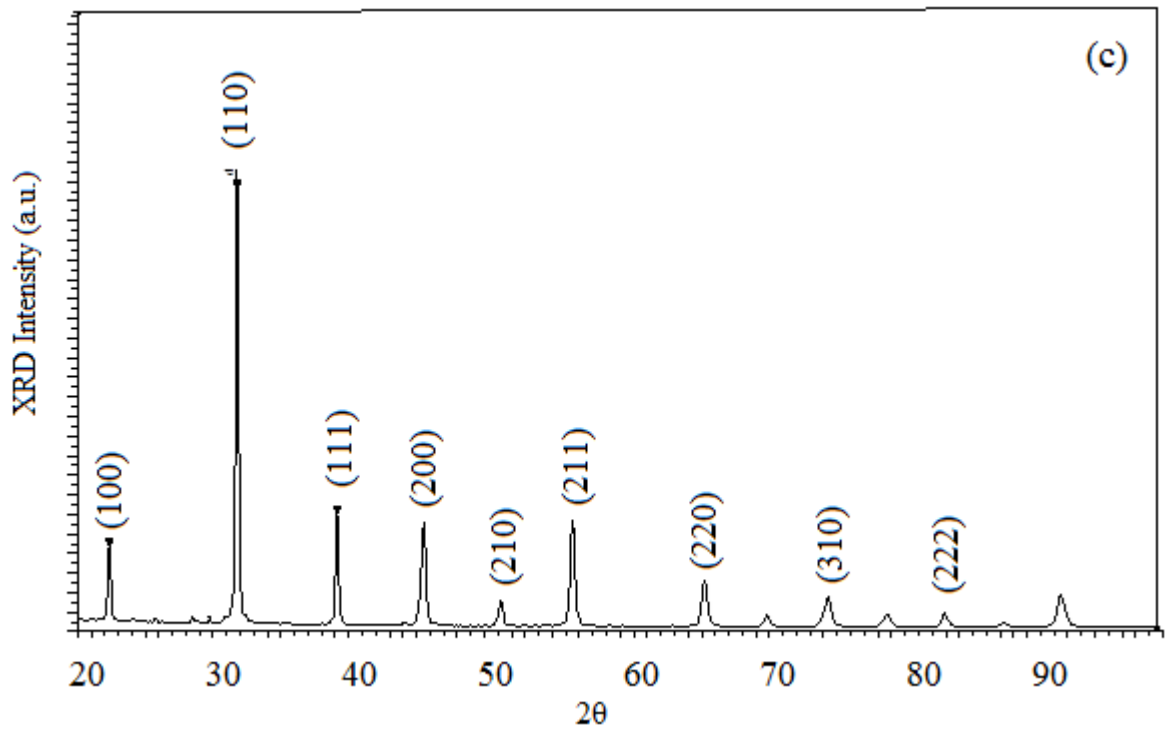

Figure 3.1(c) XRD diffractogram of $Ba_{0.85}\ Sr_{1.5}\ TiO_3$

XRD Diffractogram shows some extra weak diffraction peaks besides the peaks corresponding to standard BST chart. It has been earlier reported that during sol-gel synthesis of barium titanium oxides several intermediate phases form before the transformation of the amorphous phase into perovskite phase. The peaks were identified, as $(Ba,Sr)CO_3$ including $BaCO_3$, $SrCO_3$ and intermediate phases of the $(Ba,Sr)_2\ Ti_2\ O_5CO_3$ including $Ba_2Ti_2O_5CO_3$ [26,27]. Based on these results the chemical equation leading to BST phase evolution is:

$$Sr(CH_3COO)_2 \longrightarrow SrCO_3$$

$$Ba(CH_3COO)_2 \longrightarrow BaCO_3$$

$$(C_3H_7O)_4\ Ti \longrightarrow TiO_2$$

$$xBaCO_3 + (1\text{-}x)SrCO_3 + TiO_2 \longrightarrow Ba_xSr_{1-x}TiO_3 + CO_2$$

3.2 SEM Analysis

SEM micrograph of Barium Strontium Titanate for different compositions is shown in the fig.3.2. The average grain size of $Ba_{0.5}Sr_{0.5}TiO_3$ was found to be 3.04 micrometer, for $Ba_{0.7}Sr_{0.3}TiO_3$ was found to be 1.9 micrometer, for $Ba_{0.85}Sr_{0.15}TiO_3$ was found to be 1.3 micrometer.

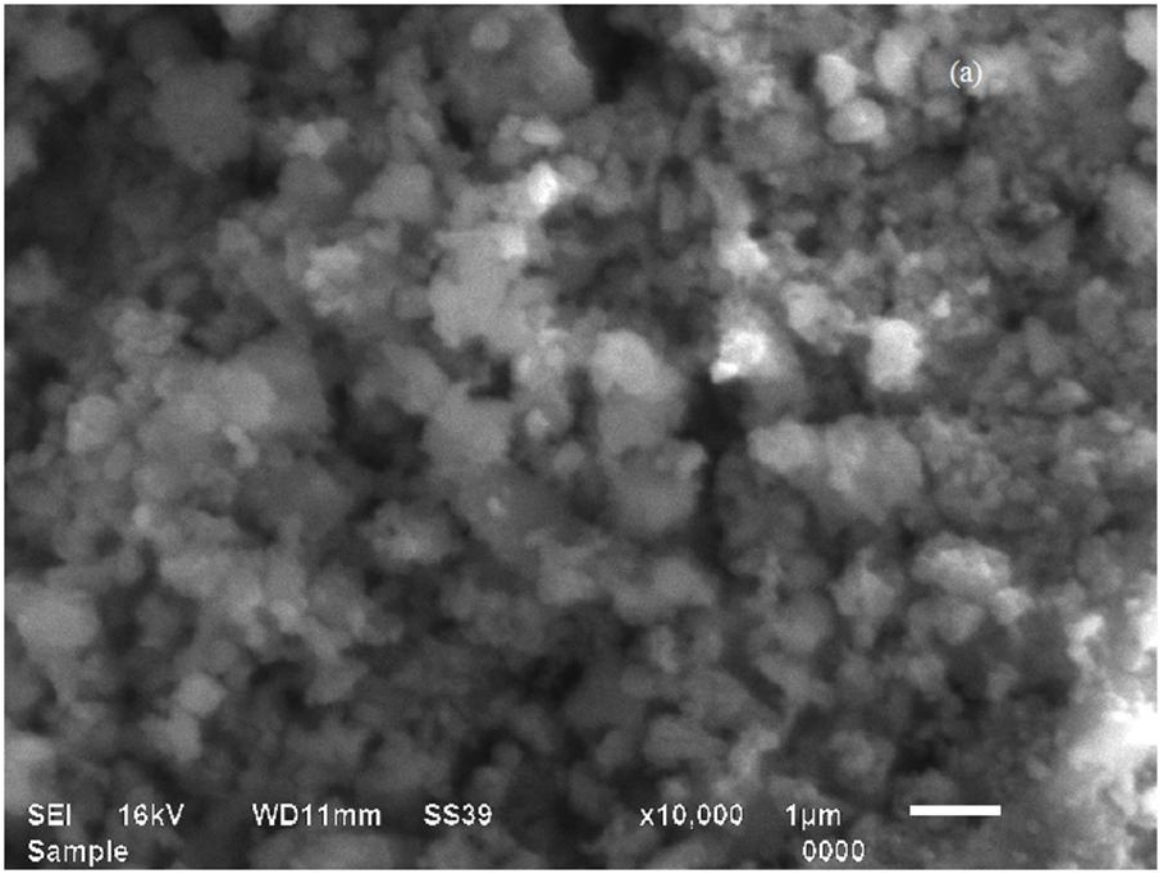

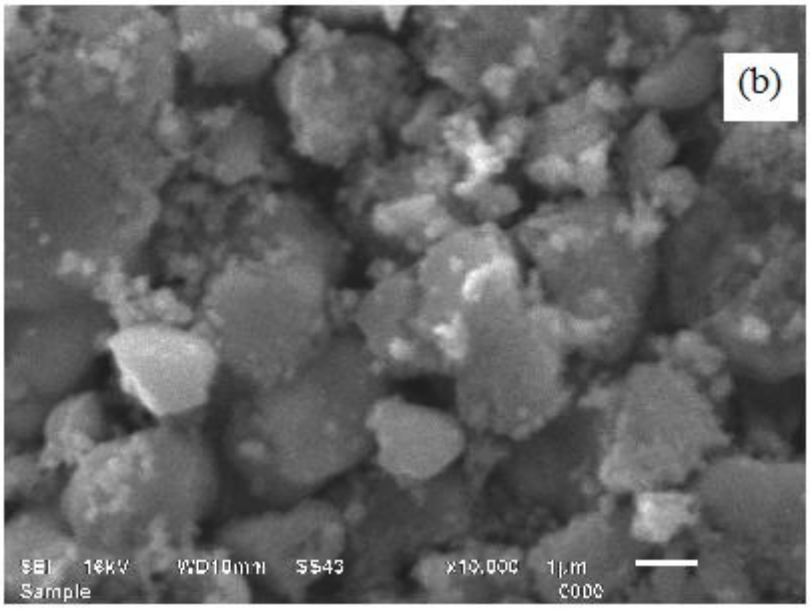

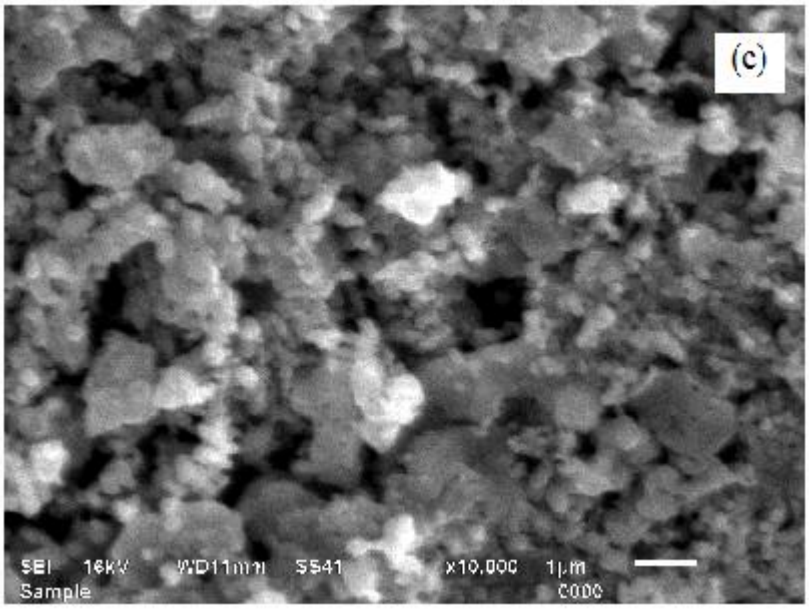

Figure 3.2: SEM (Scanning Electron Microscope) micrograph images of (a) $Ba_{0.5}Sr_{0.5}TiO_3$ (b) $Ba_{0.7}Sr_{0.3}TiO_3$ (c) for $Ba_{0.85}Sr_{0.15}TiO_3$

3.3 Electron dispersive X-ray spectroscopy (EDXS) Analysis

To find the elements present in the sample fabricated, EDXS (Energy-dispersive X-ray spectroscopy) was performed on the samples along with SEM analysis.

Fig 3.3 (a), (b) shows the EDXS spectrum of $Ba_{0.5}Sr_{0.5}TiO_3$ and $Ba_{0.85}Sr_{0.15}TiO_3$ respectively.

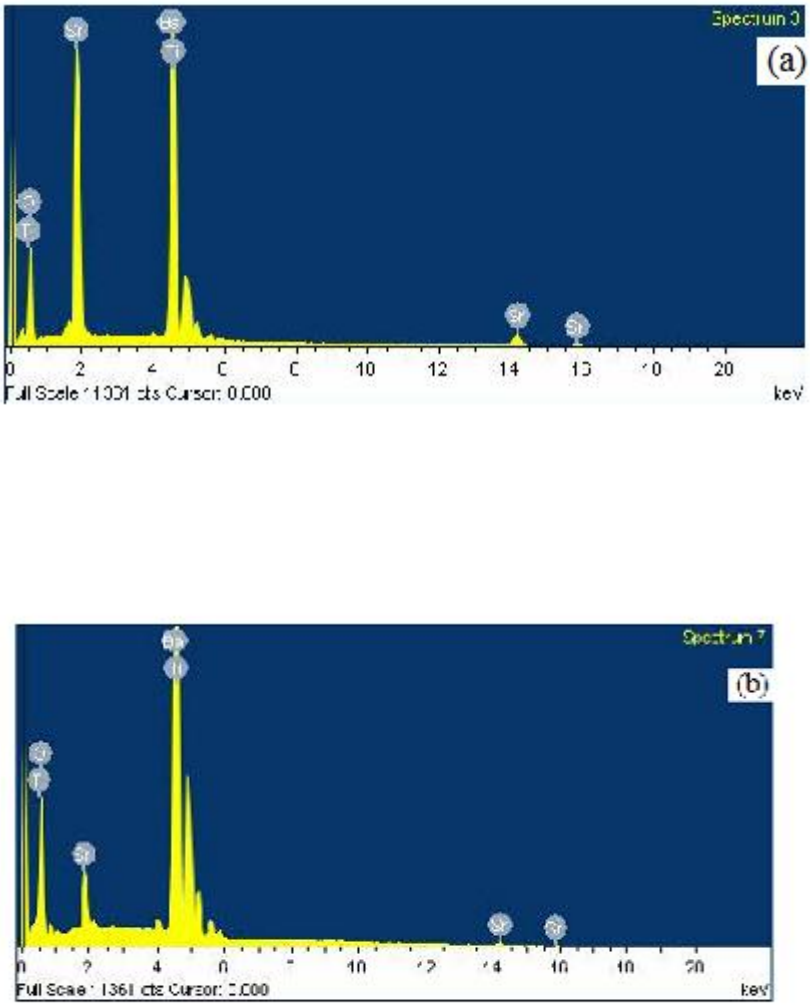

Figure 3.3 EDXS spectrum of (a) $Ba_{0.5}Sr_{0.5}TiO_3$ (b) $Ba_{0.85}Sr_{0.15}TiO_3$

The stoichiometric composition of Titanium and Oxygen is remaining close to 1:3 for all the sample. The stoichiometric composition of Barium and Strontium is changing corresponding

to the value of x, while the ratio of sum of stoichiometric compositions of Barium and strontium with Titanium was found to be =1.148 (for x= 0.5), 1.08 (for x=0.7) and 0.98 (for x=0.85), which is very close to 1 is summarisied in table below

Composition	Ratio of (Ba+Sr)/Ti
$(Ba_{0.5}Sr_{0.5}TiO_3)$	1.148
$(Ba_{0.7}Sr_{0.3}TiO_3)$	1.08
$(Ba_{0.85}Sr_{0.15}TiO_3)$	0.98

Table: Ratio of atomic percentage of Barium and Strontium with Titanium.

3.4 Dielectric Measurements

The dielectric constant of sintered sample of barium strontium titanates for different compositions as a function of frequency is shown in the fig.3.4. The obtained plots shows that there is a decrease of ε' with increase in frequency. There is a decreases of dielectric constant with increase in frequency upto 10 kHz, beyond which it almost remains constant. At low frequencies electronic, ionic, dipolar and interfacial/surface polarizations contribute to the total value of dielectric constant, but for frequencies above 10 kHz the contribution from interfacial/surface polarization gets minimized. The interfacial/surface polarization can be explained by using a Maxwell-Wagner mechanism and a Shockley-Read mechanism. The Maxwell-Wagner mechanism was concerned with interfacial polarization due to ionic motion in presence of an electric field.

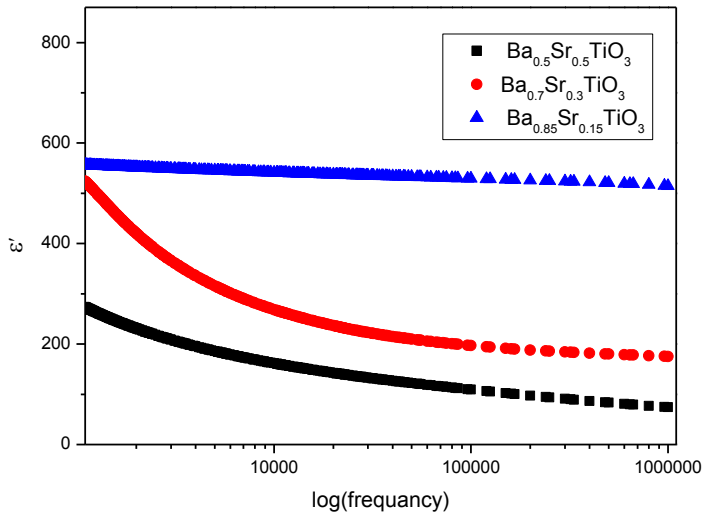

Figure 3.4: Variation of dielectric constant with frequency for different compositions.

Loss tangent is a parameter of dielectric materials that quantifies the inherent dissipation of electromagnetic energy. With increase in frequency the loss factor is found to decrease for all the compositions as shown in following figure. 3.5

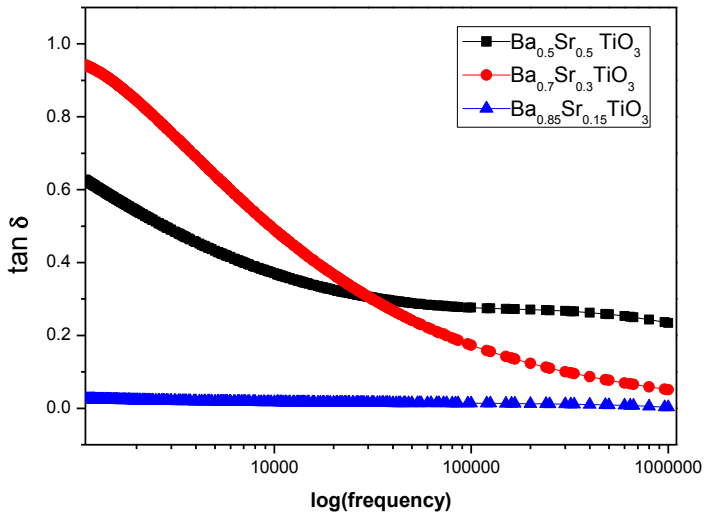

Figure 3.5: Variation of Loss Tangent with frequency for different composition.

Fig.3.6, 3.7, 3.8 shows the variation of dielectric constant with temperature at different frequencies. A significant rise in the value of dielectric constant has been found to occur for all the compositions only at lower frequencies, which is seemingly due to interfacial/ surface polarisation at the grain boundaries. But after this temperature, only for $Ba_{0.85}Sr_{0.15}TiO_3$ sample a peak in dielectric constant is noticed at temperature ~ 107 ^{0}C and after this temperature dielectric constant decreases with decrease of temperature. This type of behaviour is characteristic feature of ferroelectric material. On the other hand the other two stoichiometric compositions such as $Ba_{0.5}Sr_{0.5}TiO_3$ and $Ba_{0.7}Sr_{0.3}TiO_3$ are paraelectric.

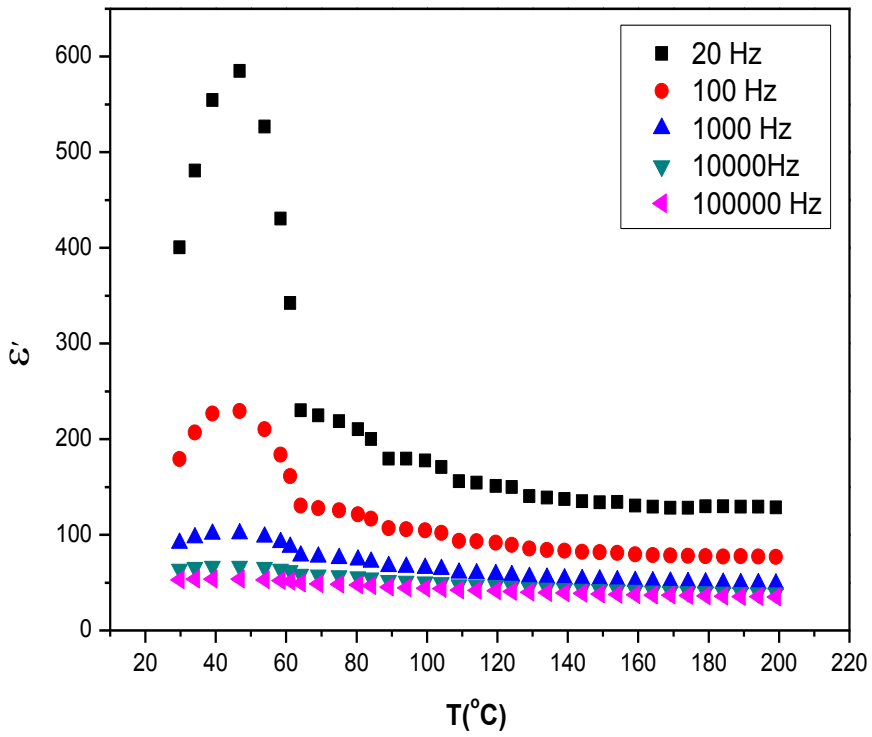

Figure 3.6: Variation of dielectric constant with temperature at different frequency

For $Ba_{0.5}Sr_{0.5}TiO_3$

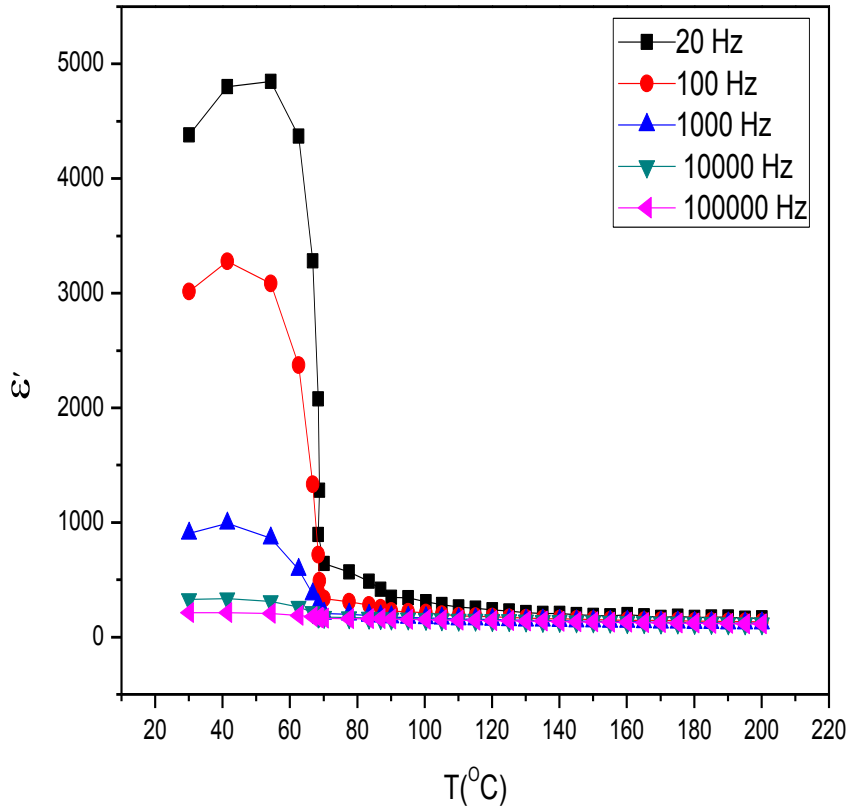

Figure 3.7: Variation of dielectric constant with temperature at different frequencies

For $Ba_{0.7}Sr_{0.3}TiO_3$

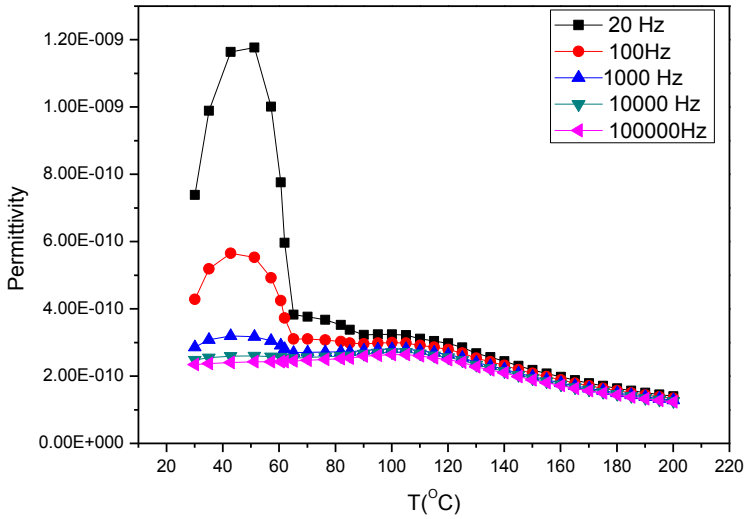

Figure 3.8: Variation of dielectric constant with temperature at different frequencies

For $Ba_{0.85}Sr_{0.15}TiO_3$

CHAPTER 4

Conclusions and Future Scope

The conclusions of characterization and synthesis are follows:

4.1 Conclusions

The discussed results in earlier chapter can be concluded as follows

i. The samples of BST with different stoichiometric compositions ($Ba_{0.5}Sr_{0.5}TiO_3$, $Ba_{0.7}Sr_{0.3}TiO_3$, $Ba_{0.85}Sr_{0.15}TiO_3$) has been successfully synthesized by Sol-Gel technique.

ii. The results of XRD analysis has confirmed the phase formation for different samples of BST. The phase of $Ba_{0.5}Sr_{0.5}TiO_3$was found to be cubic and the cell parameter was found to be a = b = c = 3.991Å. For $Ba_{0.7}Sr_{0.3}TiO_3$, the phase was found to be tetragonal and the cell parameters were found to be a = b = 3.979087, c = 3.97093Å. For $Ba_{0.85}Sr_{0.15}TiO_3$sample the phase was found to be cubic and the cell parameter was a = b = c = 3.9915Å

iii. The SEM of sintered sample has shown good surface morphology and average grain size of $Ba_{0.5}Sr_{0.5}TiO_3$was found to be 3.04 micrometer, for $Ba_{0.7}Sr_{0.3}TiO_3$was found to be 1.9 micrometer and for $Ba_{0.85}Sr_{0.15}TiO_3$stoichiometric compositions was found to be 1.3 micrometer.

iv. The results of Dielectric measurement are quite interesting. The temperature dependence of dielectric constant of different compositions of BST has shown that Only $Ba_{0.85}Sr_{0.15}TiO_3$is ferroelectric. Moreover, the value of ε' for this composition has been found to be the highest.

v. Though BST with $Ba_{0.85}Sr_{0.15}TiO_3$composition is ferroelectric but tangent los is highest.

vi. The value of ε' has been found to been to decrease with frequency, which indicates that dipoles are relaxing.

4.2 Future Scope

The BST is very promising material because of its processability and technological applicability. Therefore some further investigations are required. The future scope of this Dissertation is as follows

i. The control of grain size by different processing techniques may lead to very good dielectric and ferroelectric properties

ii. The composites of BST with some soft materials such as PVDF (Polyvinylidene fluoride) and PVA (Polyvinyl alcohol) may also be of great interesting because the ferroelectric BST can be dispersed over large area with good mechanical strength.

iii. The composites of BST with metal may also be important from physicist prospective. It may lead to various physical phenomena leading to Maxwell-Wagner effect, Interfacial polarisation effect etc.

Reference

[1]. S. J. Fiedzivsko, I.C. Hunter, T.Itoh, Y. Kobayushi, T. nishikawa, S.N.Stitzer, K. Wakino, "Dielectric materials, Devices and cicuits," IEEE Transactions Microwave Theory and Techniques, 50(2002)706-720.

[2]. A.K. Tagantsev, V.O.Sherman, K.F. Astafev, J. Venkatesh, N. Setter, "Ferroelectric materials for Microwave Tunable Applications," Journal of Electroceramics, 11(2003)5.

[3]. http://www.sia-online.org.

[4]. J.H. Jeon, J. European ceramic society, 24(2004)1045.

[5]. Mahani, R.M.; Battisha, I.K.; Aly, M.; Abou–Hamad, A.B. *J. Alloy. Compd.508 (***2010**) 354.

[6]. C. Kittel, Introduction to Solid State Physics (John Wiley and Sons, Inc. 7th ed ., 1996).

[7]. Ashcroft N.M. and N.M. Mermin, Solid State Physics, Harcourt Asia, 1st ed. (2001).

[8]. L.L. Hench and L.K. West, Principles of Electronic Ceramics, (J0hn Wiley And Sons, Inc. 1990, pp244).

[9]. Wongduan Maison, Reinhard kleeberg, Robert B. Heimann and Sukon Phanichphant," phase content, tetragonality and crystalline size of nanoscaled Barium Strontium Titanate: effect of calcination temperature" Journal European Ceramic Society, 23(2003)123.

[10]. R. Blinc, B. Zeks, "Self modes in Ferroelectric and Antiferroelectrics and related materials" Amsterdam, Elsevier. 1974.

[11]. M.E. Lines, A.M. Glass, principles and applications of Ferroelectrics and related materials, Oxford clarendon, 1977.

[12]. http://en.wikipedia.org/wiki/Phase_transition.

[13]. B. Ulrich," Dielectric properties of Polar oxides: Characterization and Imaging, Wiley, 2005.

[14]. http://en.wikipedia.org/wiki/Curie%E2%80%93Weiss_law

[15]. http://www.doitpoms.ac.uk/tlplib/dielectrics/variation.php.

[16]. http://en.wikipedia.org/wiki/Loss_tangent.

[17]. B.K Tanner et al., Applied surface science 182 (2001) 202.

[18]. Warren, X-ray Diffraction, Addison-Weslay, reading, M A, 1969.

[19]. V. Raghwan, Material Science and Engineering, PHI Learing 2004.

[20]. http://www.purdue.edu/rem/rs/sem.htm.

[21]. Joseph Goldstein, Scanning Electron Microscopy and x-ray microanalysis, Springer, 2003.

[22]. C.J. Brinker, G.W. Scherer, Sol-gel Science, The Physics and Chemistry of Sol-gel Processing, Academic Press, New York, 1990.

[23]. J.G. Cheng, X.J. Meng, J. Tang, S.L. Guo, J.H. Chu, " Fabrication and Electrical Properties of Sol-Gel Derived $Ba_{O.8}Sr_{0.2}TiO_3$ Ferroelectric film from a 0.05M spin on Solution" Applied Physics A. 70(2000)411.

[24]. Chen, J.; Zhang, Y.; Deng, C.; Dai, X. *Mater. Chem. Phy*. 121(2010)109.

[25] E. Dien, R. Verveur, M. Lejeune, A. Smith, " Preparation and properties $Ba_xSr_{1-x}TiO_3$ Thin Film Deposited by Sol-Gel Technique," Journal of Physics for Physics. 8(1998)9.73

[26] V. Somani, S. J. Kalitha, J. Electroceram, 18 (2007) 57.

[27] S. B. Majumder, M. Jain, A. Martinez, R. S. Katiyar, VanKeuls, F. A. Miranda, *J. Appl. Phys.* **2001**,*2 (90)* 896.